Soil & Tillage Research 237 (2024) 105957

Contents lists available at ScienceDirect

Soil & Tillage Research

journal homepage: www.elsevier.com/locate/still

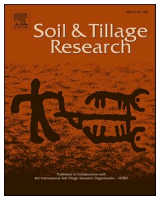

Determination of soil water retention curves from thermal conductivity curves, texture, bulk density, and field capacity

Lin Liu [a], Yili Lu [a], Robert Horton [b], Tusheng Ren [a,*]

[a] College of Land Science and Technology, China Agricultural University, Beijing 100193, China
[b] Department of Agronomy, Iowa State University, Ames, IA 50011, USA

ARTICLE INFO

Keywords:
Soil water retention curve
Van Genuchten model
Soil thermal conductivity
Field capacity
Bulk density
Soil texture

ABSTRACT

The soil water retention curve (SWRC) is frequently expressed using the van Genuchten (VG) model, which has four parameters: saturated water content (θ_s), residual water content (θ_r), α, and m (1–1/n). Soil thermal conductivity (λ), which is linked to the hydraulic properties of unsaturated soil, has been a proxy variable used to estimate SWRC. In this study, we present a new approach to estimate the VG model parameters. Parameters θ_s, α and m are calculated from the information of soil texture, bulk density (ρ_b), and a measured water content at field capacity (θ_{fc}, at −33 kPa or −10 kPa), and θ_r is estimated from the thermal conductivity versus water content curve, λ(θ), based on similarities between SWRCs and λ(θ) curves. The new approach was evaluated with laboratory and field measurements on 23 soils of various textures, ρ_b values, and θ values. Results showed that for repacked core samples, intact core samples, and in situ field soils, the new approach estimated SWRCs with average root mean square errors (RMSEs) of 0.042, 0.030, and 0.049 m^3 m^{-3}, respectively. The new approach offers a quick and effective way to estimate SWRCs accurately with measured λ(θ) curves, texture, bulk density, and θ at field capacity.

1. Introduction

An accurate soil water retention curve (SWRC) is necessary to effectively model water flow and solute transport in soils (Colman, 1947; Vogel and Cislerova, 1988; Kirkham, 2005). Currently, a limited number of techniques available for measuring SWRCs over the full water content range. For example, the sandbox apparatus imposes suctions on soil samples in the matric potential range of 0 to -10 kPa (Gupta and Larson, 1979), while the pressure plate extractor typically operates in the matric potential range from -10 to -1500 kPa (Dane and Hopmans, 2002). Additionally, the pressure plate method has the drawbacks of being time consuming and having potential errors from poor soil-plate contact, low ceramic plate conductance, and soil volume changes in the dry range (Bittelli and Flury, 2009). It is also acknowledged that most of the available methods are limited to specific sample sizes (Mohammadi and Vanclooster, 2011).

Many empirical and semi-physical pedotransfer functions (PTFs) have been developed to estimate SWRCs from easily accessible soil properties such as particle size distribution (PSD), bulk density (ρ_b), and organic matter (OM) content (Wösten et al., 1999; Schaap and Leij, 1998, 2000; Børgesen et al., 2008; Weynants et al., 2009). Arya and Paris (1981) developed a semi-physical PTF to estimate SWRCs based on the similarity between the shapes of the PSD curve and the SWRC. The performance of this model depends strongly on the number and range of points within the datasets that are used in the model derivation. Mohammadi and Vanclooster (2011) improved the Arya and Paris (1981) approach by dividing the PSD into n size fractions and assuming the soil particles in each size fraction are spherical. This model underestimates water content in the dry range due to the simplified treatment of the soil pore system (Mohammadi and Vanclooster, 2011). Several SWRC models, such as the Brooks and Corey (1964) model, the Gardner (1970) model, the van Genuchten (VG) (1980) model, and the Fredlund and Xing (1994) model, have been developed. Model parameters are generally obtained by fitting the models to measured values on the SWRC or they are derived from PTFs that use easily measured soil properties (Zhai et al., 2012; Chen et al., 2014; Fu et al., 2021a, 2021b).

It has long been recognized that there are similarities between water flow and heat transfer in porous media: 1) Both processes are influenced by similar factors (e.g., texture, porosity, and θ) and can be described by the percolation theory (Ghanbarian et al., 2015; Lu et al., 2019; Fu et al., 2021b); 2) The models used to describe water flow and heat transfer, i.e., Darcy's law for water flow and Fourier's law for heat transfer, have

* Corresponding author.
E-mail address: tsren@cau.edu.cn (T. Ren).

https://doi.org/10.1016/j.still.2023.105957
Received 4 February 2023; Received in revised form 3 October 2023; Accepted 14 November 2023
Available online 30 November 2023

similar forms. Thus, researchers have attempted to establish relationships between soil thermal conductivity (λ) and matric potential of soil water (*h*) (McCumber and Pielke, 1981; Reece, 1996; Nichol et al., 2003; Lu et al., 2015; Kroener et al., 2018; Lu et al., 2019; He et al., 2020; Fu et al., 2021b). Likos (2014) proposed an approach to estimate λ(θ) curves from SWRC measurements for coarse-textured soils based on the similarity between a bimodal formulation of the SWRC and λ(θ) curves. Considering that both SWRCs and λ(θ) curves have a sigmoidal shape, Lu and Dong (2015) proposed a closed form model, which had a similar form to that of the VG model, to describe λ variations with θ in four water regimes, i.e., hydration, pendular, funicular, and capillary. The model parameters were determined by fitting the model to λ(θ) measurements. Fu et al. (2021b) presented a model to estimate SWRC model parameters from λ(θ) data and easily measured soil properties (i.e., texture, ρ_b, and organic carbon content). An independent validation on repacked soil samples showed that the Fu et al. (2021b) approach provided satisfactory results. Nonetheless, the above-mentioned approaches to determine SWRCs from λ(θ) data have not been tested with in situ soil observations.

This study aims to introduce a new approach to estimate SWRCs from λ(θ) curves combined with the θ value at field capacity (−33 kPa or −10 kPa), soil bulk density, and texture information. The new approach is tested with *h* and λ data obtained on repacked, and intact soil cores, and on in situ field measurements.

2. Model development

2.1. The similarity between λ(θ) curves and SWRCs

Fig. 1 presents a conceptual SWRC and a λ(θ) curve for a typical fine-textured soil. The SWRC and λ(θ) curve are partitioned into three general regimes along the path of decreasing θ in the unsaturated domain: (1) the wet range (i.e., Regime I), when the soil is nearly saturated, (2) the menisci range (i.e., Regime II), when the capillary water decreases gradually and the film water increases progressively (Lu and Likos, 2004; Ewing and Horton, 2007), and (3) the dry range (i.e., Regime III), when the capillary air-water interface diminishes steadily and the liquid system is characterized by an isolated and discontinuous water phase.

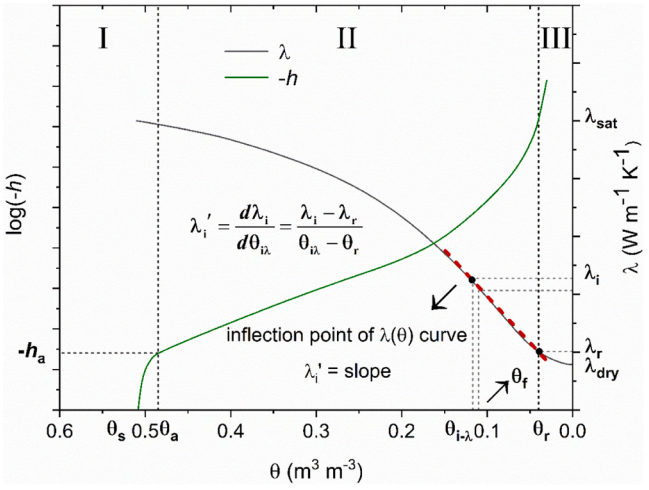

Fig. 1. Conceptual diagram of a typical soil water retention curve (SWRC) and a thermal conductivity (λ) curve for a fine-textured soil. The vertical black dot lines represent the boundaries between Regimes I, II, and III. The red dot line is drawn across two black points with slope λ_i' (where the right point represents the thermal conductivity at the residual water content (θ_r, λ_r) and the left point represents the inflection point ($\theta_{i\lambda}$, λ_i) (i.e., the λ at which the curvature of λ(θ) curve is 0). Parameters λ_{sat} and λ_{dry} are the thermal conductivity values of saturated and dry soil, θ_f is Lu and Dong (2015) model parameter, θ_a and h_a are the water content and matric potential at the air-entry condition.

In Regime I, the soil system is nearly saturated, and it requires little energy to remove water because the surface and capillary forces have negligible effects on water molecules at or close to saturation. As θ decreases from saturation to the value of air-entry matric potential (θ_a, h_a), the magnitude of -*h* increases dramatically from 0 to -h_a (Fig. 1). However, in this θ range, the λ value is close to the thermal conductivity at saturation (λ_{sat}) and remains relatively stable because the loss of liquid heat-transfer pathways has a negligible effect on λ_{sat}.

At the onset of the menisci range (or Regime II), water loss occurs from large pores as the capillary force (-*h*) increases gradually, while a rapid λ decrease appears because of the reduction of contacts among solid particles (Fig. 1). The drying process continues until θ reaches a critical point at which all capillary water has escaped, the liquid pathways for heat transfer are lost completely, and thus heat transfer shifts to film water (Lu and Likos, 2004; Ewing and Horton, 2007; Lu and Dong, 2015). The rates of -*h* increase and λ decrease reach the maximum values at the end of the menisci range. In Regime III, water is bound strongly by intermolecular forces due to the Van der Walls forces, water-solute-clay interactions and electrostatic interactions between solid surfaces and water dipoles, thus, the water molecules and solutes on the soil mineral surfaces are essentially immobile (Lu and Likos, 2004; Pozdnyakov et al., 2006; Lu et al., 2015). The dipolar molecules of adsorbed water create a conductive path in the soil matrix. With θ values decrease from the residual water content (θ_r) to oven-dry, the corresponding *h* value decreases rapidly to -10^6 kPa (Nitao and Bear, 1996; Likos, 2014), and the λ values decrease from the λ at θ_r (λ_r) to the λ of dry soil (λ_{dry}) (Pozdnyakov et al., 2006; Likos, 2014).

From the conceptual linkage between matric potential and thermal conductivity dynamics with water content, it is reasonable to assume that there exists a similarity between the SWRC and λ(θ) curve, and it is possible to link the two curves quantitatively. In this study, we use the van Genuchten (1980) model to describe SWRCs,

$$\theta(\Theta) = \frac{\theta - \theta_r}{\theta_s - \theta_r} = [1 + (-\alpha h)^n]^{-m} \quad (1)$$

where θ(Θ) is the normalized θ, θ_s is the saturated water content ($m^3\ m^{-3}$), θ_r is the residual water content ($m^3\ m^{-3}$), α (> 0, cm^{-1}) is related to the inverse of the air-entry pressure, *m* (0 < *m* < 1) is a pore-size distribution parameter, and *n* = 1/(1-*m*) (*n* > 1). Values of the four parameters, θ_s, θ_r, α, and *m*, are usually determined by fitting Eq. (1) to SWRC measurements.

The θ_s value is assumed to be equal to the soil porosity, which is calculated as,

$$\theta_s = \phi = 1 - \frac{\rho_b}{\rho_s} \quad (2)$$

where ϕ is soil porosity, ρ_s is soil particle density, assumed to be 2.65 g cm^{-3}.

The parameter θ_r is normally treated as the water content at which soil hydraulic conductivity approaches 0 or is assumed to be the water content below which liquid water becomes discontinuous and there is no continuous liquid water flow in the soil (van Genuchten et al., 1991; Fu et al., 2021b). The value of θ_r depends mostly upon the surface area of soil particles, which is mainly determined by clay content (f_{clay}) and mineralogy (Tuller and Or, 2005; Poeplau et al., 2015). There are reports that ρ_b has only a small effect on θ_r (Assouline, 2004; Tian et al., 2018). For measurements, the θ_r value is also affected by the patience of the experimenter, and the ability of the equipment to avoid artifacts over long-time measurement periods. Chen et al. (2014) assumed that θ_r was about the water content at log(-*h*) = 5 because θ_r represented the θ at low matric potential values (< −1500 kPa) at the dry end of the SWRC where dθ/dh ≈ 0 (Minasny et al., 1999). Fu et al. (2021a) introduced an empirical equation to estimate θ_r,

$$\theta_r = \left(0.0033 f_{clay} + 0.007\right)\frac{\rho_b}{\rho_w} \tag{3}$$

where ρ_w is the density of water, assumed to be 1.0 g cm^{-3}.

Based on the sigmoidal shapes of SWRCs and λ(θ) curves, Lu and Dong (2015) developed a unified conceptual λ(θ) model, which had a form similar to the van Genuchten (1980) SWRC model. The λ(θ) curve is described as,

$$\lambda(\Lambda) = \frac{\lambda - \lambda_{dry}}{\lambda_{sat} - \lambda_{dry}} = 1 - \left[1 + \left(\frac{\theta}{\theta_f}\right)^{\frac{1}{1-p}}\right]^{-p} \tag{4}$$

where λ(Λ) is the normalized thermal conductivity, θ_f is the water content at the onset of the funicular water regime, p is defined as the pore fluid network connectivity parameter that can also be related to the pore-size parameter m in the van Genuchten SWRC model, λ_{sat} and λ_{dry} are the thermal conductivity values (W m^{-1} K^{-1}) of saturated and dry soils, respectively.

The values of λ_{sat} and λ_{dry} can be estimated from easily measured soil properties. A geometric mean equation based on the thermal conductivity of water (λ_w = 0.594 W m^{-1} K^{-1} at 20 °C) and effective thermal conductivity of soil solids (λ_s), is used to estimate λ_{sat} (Johansen, 1975; Lu et al., 2007),

$$\lambda_{sat} = \lambda_s^{\,1-\phi}\lambda_w^{\phi} \tag{5}$$

where λ_s is determined using another geometric mean equation from the quartz content (q, which is assumed to be equal to the volume fraction of sand), and thermal conductivity values of quartz (λ_q = 7.7 W m^{-1} K^{-1}) and of other minerals (λ_o),

$$\lambda_s = \lambda_q^{q}\lambda_o^{1-q} \tag{6}$$

where λ_o is taken as 2.0 W m^{-1} K^{-1} for soils with quartz content $q > 0.2$, and 3.0 W m^{-1} K^{-1} for soils with $q \le 0.2$ (Johansen, 1975).

Lu et al. (2007) introduced the following equation to estimate λ_{dry} from soil porosity (ϕ),

$$\lambda_{dry} = 0.51 - 0.56\phi \tag{7}$$

Once the λ_{sat} and λ_{dry} values are estimated by using Eqs. (5–7), parameters θ_f and p can be obtained by fitting Eq. (4) to a measured λ-θ dataset.

2.2. New approach to obtain the θ_r value from λ(θ) curve

In this study, we introduce a graphical method to determine the θ_r value from a λ(θ) curve. First, the Lu and Dong (2015) parameters are estimated by fitting Eq. (4) to the measured λ(θ) curves. Then, the inflection point ($\theta_{i\lambda}$, λ_i) on the λ(θ) curve is identified by locating the $\theta_{i\lambda}$ value at which the maximum slope (λ_i') occurs (Fig. 1). Assuming that the tangent line across the inflection point also goes through the point at the residual water content (θ_r, λ_r), the λ_i' of the λ curve is expressed as,

$$\lambda_i' = \frac{\lambda_i - \lambda_r}{\theta_{i\lambda} - \theta_r} = \frac{d\lambda_i}{d\theta_{i\lambda}} \tag{8}$$

Appendix A presents the steps used to determine $\theta_{i\lambda}$, λ_i, and λ_r values using the Lu and Dong (2015) λ model. An implicit function for θ_r is derived by simplifying Eq. (8),

$$\left[1 + \left(\frac{\theta_r}{\theta_f}\right)^{\frac{1}{1-p}}\right]^{-p} = (1+p)^{-p} + \left(\theta_f p^{1-p} - \theta_r\right)\left(\frac{p}{1+p}\right)^{p+1}\frac{\theta_f{}^{-1}}{1-p} \tag{9}$$

Clearly, θ_r is a function of parameters θ_f and p, both of which can be estimated by fitting Eq. (4) to measured λ-θ values. In this study, we solved Eq. (9) by applying the SOLVE function in MATLAB (version 2019 for Windows).

For convenience, we used the Lu et al. (2007) λ model to obtain the complete λ(θ) curve, rather than using actual measurements. In the Lu et al. (2007) model, the normalized soil thermal conductivity is expressed as,

$$\lambda(\Lambda) = \frac{\lambda - \lambda_{dry}}{\lambda_{sat} - \lambda_{dry}} = \exp\left\{B\left[1 - \left(\frac{\theta}{\theta_s}\right)^{B-1.33}\right]\right\} \tag{10}$$

where B is a soil texture dependent parameter (0.96 for coarse-textured soils with $q > 0.4$, and 0.27 for fine-textured soils with $q \le 0.4$).

2.3. Determination of parameters α, m, and n (or 1/(1-m))

In this study, the SWRC is expressed as a function between θ and log (-h). We first determined the slope of the SWRC in a similar way to that of the λ(θ) curve (Appendix B). Then the slope (θ_i') at the inflection point (where the modulus of slope reaches its maximum) of the SWRC is obtained,

$$\theta_i' = -n(\theta_s - \theta_r)\frac{\ln(10)}{\left(1+\frac{1}{m}\right)^{m+1}} = \frac{(\theta_s - \theta_r)\left[1 - \left(1+\frac{1}{m}\right)^{-m}\right]}{\log(-h_a) + \log\alpha + \frac{1}{n}\log m} \tag{11}$$

where θ_{ih} and h_i are the water content and matric potential values at the inflection point, respectively. Parameter h_a, the air-entry matric potential, is approximated from the intersection of the tangent line across the inflection point and horizontal line across θ_s (Fredlund and Xing, 1994; Zhai and Rahardjo, 2012; Fu et al., 2021b).

Fu et al. (2021a) developed an empirical relationship between α and h_a,

$$\alpha = 0.3(-h_a)^{-0.79} \tag{12}$$

Combining Eqs. (11) and (12), the following relationship is obtained,

$$\left(1 - \frac{1}{\left(1+\frac{1}{m}\right)^{m}}\right)\frac{1}{(m-1)\log(m) + 0.26\log(\alpha) - 1.26\log(0.3)} = \frac{1}{1-m}\frac{\ln(10)}{\left(1+\frac{1}{m}\right)^{m+1}} \tag{13}$$

In general, field capacity is defined as the amount of water held in a soil after excess gravitational water has drained away (Veihmeyer and Hendrickson, 1931). The θ and h values at field capacity (θ_{fc}, h_{fc}) are particularly sensitive to variations in parameter m (Tian et al., 2018). Thus, it is reasonable to use the θ_{fc} and h_{fc} values to estimate α or m using Eq. (1) if one of them is known,

$$\frac{\theta_{fc} - \theta_r}{\theta_s - \theta_r} = \left[1 + \left(-h_{fc}\alpha\right)^n\right]^{-m} \tag{14}$$

Colman (1947) proposed a static h_{fc} value of − 33 kPa for all soils. However, many studies have shown that h_{fc} varies strongly with soil texture (Veihmeyer and Hendrickson, 1931; Miller and Klute, 1967; Assouline and Or, 2014). Generally, coarse-textured soils readily drain due to the large ratio of macropores to micropores, thus have relatively large h_{fc} values. In this study, we select an h_{fc} value of − 10 kPa for coarse-textured soils and an h_{fc} value of − 33 kPa for fine-textured soils.

Once the water content at field capacity (θ_{10} or θ_{33}) is known, parameters α and m can be determined by solving Eqs. (13) and (14). In practice, the PLOT function in MATLAB can be used to draw its image, and the GINPUT function can be used to locate the intersection coordinates, i.e., the unknown values of α and m.

Fig. 2 summarizes the process used to determine the four VG model parameter values.

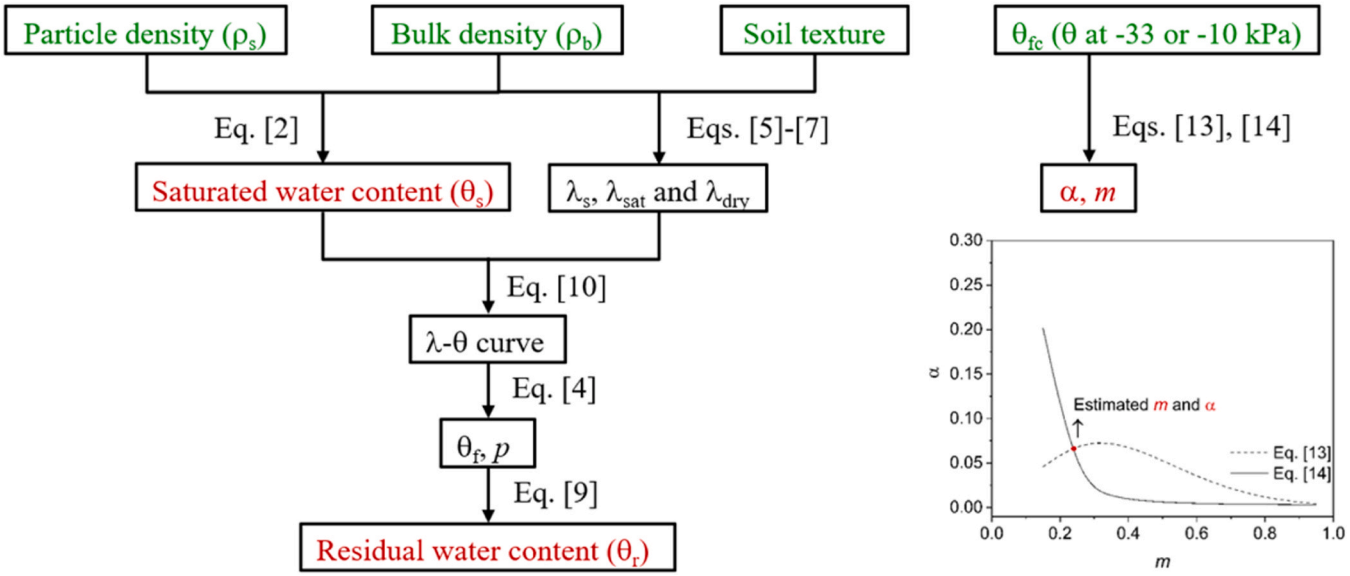

Fig. 2. The process used to determine VG model parameter values for θ_s, θ_r, α, and m (or n). Here h represents the matric potential of soil water; λ, λ_s, λ_{sat}, and λ_{dry} are thermal conductivity values of bulk soil, soil solids, saturated soil, and dry soil, respectively; θ_f and p are parameters of the Lu and Dong (2015) λ model; and θ_{fc} is the water content at field capacity. The input parameters are labeled in green color, and the target parameters are labeled in red. The figure on the right depicts an example solution for parameters α and m.

3. Materials and Methods

Table 1 lists the basic physical properties of the 23 soils examined in this study. The sand content ranges from 0.02 to 1.00 g g^{-1} and the clay content ranges from 0.00 to 0.55 g g^{-1}. Published SWRC data for 20 soils with a wide range of textures and ρ_b values along with new measurements for another 3 soils were used to validate the model. The new measurements, including laboratory and field experiments, were performed to collect (θ, h) data in soils with different textures and bulk density values. Data for the first 15 soils (Table 1) were obtained from repacked soil columns, while data for the remaining 12 soils were obtained from intact soil cores. Soils 1–3 were used for both repacked and intact soil measurements, and Soil 1 was also used in an in-situ field study during a maize growing season. For the new measurements on repacked soil columns, the soil samples were air-dried, ground, and sieved through a 2-mm screen before packing. Soil particle size

Table 1
Texture, particle size distribution (PSD), bulk density (ρ_b), and sources of the 23 used soils in the study.

	Soil Code	Texture	PSD			ρ_b	Sources
			2–0.05 mm	0.05–0.002 mm	< 0.002 mm		
			g g^{-1}			Mg m^{-3}	
Repacked soil cores	1	silty clay loam	0.24	0.45	0.31	1.20, 1.30, 1.40	This study
	2	silt loam	0.27	0.50	0.23	1.35, 1.45, 1.55	
	3	loamy sand	0.83	0.11	0.06	1.55, 1.60, 1.70	
	4	sand	0.93	0.01	0.06	1.60	Lu et al. (2008)
	5	sandy loam	0.67	0.21	0.12	1.41	
	6	silty clay loam	0.19	0.54	0.27	1.29	
	7	silt loam	0.11	0.70	0.19	1.33	
	8	silty clay loam	0.08	0.60	0.32	1.32	
	9	silt loam	0.02	0.73	0.25	1.20	
	10	sand	0.91	0.07	0.02	1.65	Jensen et al. (2015)
	11	loamy sand	0.81	0.14	0.05	1.59	
	12	sandy loam	0.74	0.17	0.09	1.58	
	13	loam	0.27	0.50	0.23	1.39	
	14	clay	0.30	0.18	0.51	1.43	
	15	sandy clay loam	0.49	0.21	0.30	1.51	
Intact soil cores	1(N)	silty clay loam (No-till)	0.24	0.45	0.31	0.98, 1.21, 1.38, 1.41, 1.45	This study
	1(R)	silty clay loam (Ridge-till)	0.24	0.45	0.31	1.27, 1.45, 1.54, 1.36, 1.49	
	2	silt loam	0.27	0.50	0.23	1.02, 1.03, 1.16, 1.46, 1.52	
	3	loamy sand	0.83	0.11	0.06	1.41, 1.48, 1.58, 1.60	
	16	Fontainebleau sand	1.00	0.00	0.00	1.67	Doussan and Ruy (2009)
	17	Avignon silty clay loam	0.16	0.51	0.33	1.64	
	18	Collias loam	0.38	0.49	0.14	1.49	
	19	silt loam	0.29	0.55	0.16	1.56	Schelle et al. (2013)
	20	silt	0.07	0.83	0.10	1.40	
	21	silty clay	0.02	0.53	0.45	1.40	Nemes et al. (1999)
	22	loam	0.45	0.38	0.17	1.25	Fu et al. (2011)
	23	clay	0.07	0.36	0.55	1.48	
Field measurement	1	silty clay loam	0.24	0.45	0.31	1.26–1.40	This study

distribution was determined with the pipette method (Gee and Or, 2002).

In addition, we used literature data for the repacked soils reported by Lu et al. (2008) (Soils 4–9) and Jensen et al. (2015) (Soils 10–15). The SWRC measurements on intact soil cores from Doussan and Ruy (2009) (Soils 16–18), Schelle et al. (2013) (Soils 19–20), Nemes et al. (1999) (Soil 21), and Fu et al. (2011) (Soils 22–23) were used to evaluate the new approach developed in this study.

3.1. Measurements on repacked soil samples at various water contents

For Soils 1–3, laboratory SWRC measurements were made on soil cores (50-mm inner diameter and 50-mm in height) that were repacked to selected ρ_b values. Three replicated cores were prepared at each ρ_b. The soil columns were saturated slowly with distilled water, and then used for SWRC measurements in a sandbox (with h values of −0.5, −0.75, −1.5, −4, −6, and −8 kPa) and a pressure plate apparatus (with h values of −10, −30, −70, −100, −300, and −500 kPa). After equilibration at each specific h value, the sample mass was recorded, and the θ value was measured with the TDR technique. Briefly, a TDR sensor (45-mm long, 2-mm in needle diameter, and 8-mm needle-to-needle spacing), connected to a TDR200 device (Campbell Scientific Inc., Logan, UT), was inserted into each column vertically from the soil surface to determine θ (Liu et al., 2008). To avoid the potential effect of the TDR sensor on soil structure (and thus on measured θ and h data), an individual soil core was prepared for each h value. After imposing the lowest h value, the samples were oven-dried at 105 ℃ for 48 h to determine the dry mass and water content.

3.2. Measurements on intact soil samples at various water contents

Intact soil columns (Soils 1–3) were collected at three field sites in Lishu County, Jilin Province, China. The soil textures were silty clay loam, loamy sand, and silt loam for sites 1, 2, and 3, respectively (Table 1). Soil samples collected in no-till and ridged plots are labeled N and R, respectively. At each site, intact soil samples were collected from the 0–5, 5–10, 10–15, 20–25, and 30–35 cm soil layers with stainless steel cylinders (5-cm high and 5-cm in diameter) to determine ρ_b and θ. Three replicated samples were collected in each soil layer.

For soil water retention curve measurements, intact soil samples were collected with cylindrical stainless-steel rings (1-cm high and 5-cm in diameter) from the 0–5, 5–10, 10–20, 20–30, and 30–40 cm soil layers. Three replicated cores were obtained in each soil layer. The samples were tightly wrapped with plastic film, brought to the laboratory, and then slowly saturated, and soil water retention curves were measured with sandbox equipment (−0.25, −1, −2, −5, −8, and −10 kPa) and a pressure plate apparatus (−50, −100, −300, −500, and −1500 kPa). The sample masses were recorded after equilibration at each matric potential. After reaching an equilibration at − 1500 kPa, the samples were dried at 105 ℃ for 48 h to determine the dry mass, which was used to calculate the θ at each h value.

The accuracy of SWRC measurements is scale dependent (Jalbert and Dane, 2001; Yan et al., 2022). When measuring SWRCs using the sandbox and pressure plate, the measured θ and h data are assumed to be the mean values of the sample. In reality, θ and h may distribute non-uniformly throughout the sample. The h assigned to the soil column is the pressure applied on the pressure plate, rather than the representative h, while the corresponding θ is the water content of the bulk soil column (Jalbert and Dane, 2001; Ewing et al., 2015; Yan et al., 2022). Studies have shown that as the sample height decreases, the SWRC becomes sharper at high saturation (Hunt et al., 2013). In this study, we obtained the representative h value of the bulk column from measured data following the approach of Jalbert and Dane (2001) (their Eq. (7), Appendix C).

3.3. In situ field measurements

In situ field measurements were performed on the clay loam soil (Soil 1) at the Lishu Experimental Station of China Agricultural University (43°16′ N, 124°26′ E), located in Lishu County, Jilin Province, China. To facilitate sensor installation, we made a small trench (about 150-mm long, 150-mm wide, and 150-mm deep), and pushed the TDR sensor (70-mm long, 2-mm in diameter, and 10-mm needle-to-needle spacing) horizontally into the soil at the depth of 100 mm. A TDR200 system, which was controlled with a datalogger (model CR3000, Campbell Scientific Inc., Logan, UT), measured θ values every 60 min. Meanwhile, a matric potential sensor (TensioMark, ecoTech Umwelt-Meßsysteme, GmbH, Bonn, Germany), with a length, width, and thickness of 130, 20, and 7 mm, respectively, was installed at the 100-mm depth at a distance about 50 mm away from the TDR sensors to monitor the dynamics of h. The TensioMark sensors were covered with wet native soil before installation, and then inserted diagonally into a pre-made slot at the desired depths. The TensioMark sensors were controlled with a datalogger (SDI-12, enviLog, Germany) via SDI-12-multiple sockets. Finally, intact soil cores were collected nearby the TensioMark sensors with ring samplers (50-mm in diameter and 50-mm high) at the 100-mm depth to determine the actual ρ_b and θ values on DOYs 150, 176, and 197. The field observations covered an 85-day period in 2020. A weather station at the site monitored the rainfall, air temperature, and wind speed.

3.4. Model validation

We evaluated the performance of the new approach to estimate SWRCs by using independent measurements on repacked soil core samples of Soils 1–15, intact core samples of Soils 1–3 and 16–23, and field measurements on Soil 1.

The estimated SWRCs were evaluated using root mean square errors (RMSE) and bias with respect to the measured values,

$$\mathrm{RMSE} = \sqrt{\frac{\sum (\theta_{\mathrm{estimated}} - \theta_{\mathrm{measured}})^2}{N}} \tag{15}$$

$$\mathrm{Bias} = \frac{\sum (\theta_{\mathrm{estimated}} - \theta_{\mathrm{measured}})}{N} \tag{16}$$

where N is the number of data pairs, $\theta_{\mathrm{estimated}}$ and $\theta_{\mathrm{measured}}$ are the estimated and measured water content values, respectively.

4. Results and Discussion

4.1. Sensitivity of estimated SWRCs to variations in model parameters

The shape of the estimated SWRC is determined by the model parameters. Here we perform a sensitivity analysis on the responses of estimated SWRCs of the sandy loam soil to variations in van Genuchten model parameters θ_s, θ_r, α, and m. As expected, the saturated soil water content, θ_s, strongly affected the wet part of the SWRC (Fig. 3(a)). Changes in parameter θ_r, mainly affected the magnitude of water content at the dry end (Fig. 3(b)). Although both parameters α and m affected the shapes of the estimated SWRCs, the influence of parameter α occurred mainly in the wet range ($\log(-h) < 2$) (Fig. 3(c)), while parameter m (or n) determined the slope of the SWRC in the $\log(-h)$ range of 1.5–2.5, i.e., an increase in m generated a sharper slope in the SWRC, while a decrease in m lessened the slope in the SWRC (Fig. 3(d)). These results agreed with Tian et al. (2018) that the shape of a SWRC was mainly dominated by parameters θ_s and α in the matric potential range of 0 to − 10 kPa.

It should be noted that parameter θ_r in the SWRC model is estimated from parameters θ_f and p in the Lu and Dong (2015) λ model. However, the Lu and Dong (2015) λ model fails to provide an accurate λ value for a saturated soil because the λ value is set to λ_{sat} and $\lambda(\Lambda)$ becomes unity,

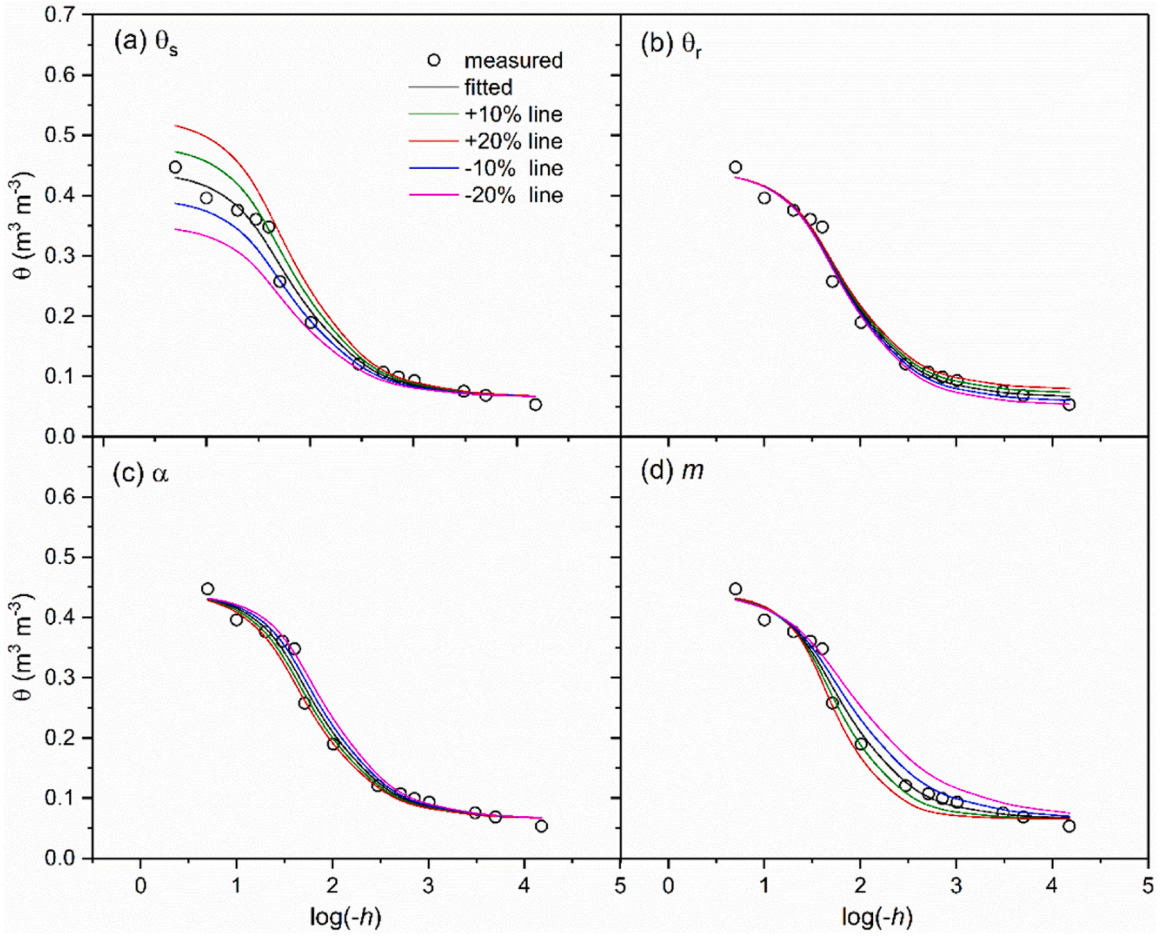

Fig. 3. The effects of parameters (a) θ_s, (b) θ_r, (c) α, and (d) *m* on sandy loam modeled soil water retention curves. The + 10%, + 20%, − 10%, and − 20% lines refer to the estimated curves using 1.1, 1.2, 0.9, and 0.8 times the corresponding parameter values, respectively.

which brings about an unrealistic situation in Eq. (4): The θ value reaches infinity instead of θ_s at λ_{sat}. Failure to capture the variation of λ in the very wet region may cause erroneous estimates of θ_f and *p*, and thus, inaccurate θ_r values. For the sandy loam soil, a 10% uncertainty in θ_f introduces a 10% error in the estimated θ_r value with Eq. (9), and a 10% uncertainty in *p* produces a 7% error in the estimated θ_r value (Fig. 3). Further sensitivity analyses shows that the larger the uncertainty in *p* and θ_f values, the larger the error in the corresponding θ_r values. However, θ_f error has a greater effect on the accuracy of θ_r estimations than did errors in *p* (Fig. 4). Additionally, uncertainties in parameter B may introduce errors in both θ_f and *p*, leading to inaccuracies in the estimated θ_r values. Our analysis indicated that for fine-textured soils, a 10% uncertainty in the B value introduces 3.4% and 0.3% errors in the fitted θ_f and *p* values, respectively; for coarse-textured soils, the corresponding errors are 39.6% and 9.8%, respectively. Thus, errors in θ_f and *p* produce erroneous θ_r values, and inaccurate SWRCs.

In addition, the accuracies of estimated parameters α and *m* are affected strongly by the reliability of field capacity (θ_{fc}, h_{fc}), because both parameters are obtained by solving Eqs. (13) and (14) simultaneously. According to Eq. (13), the relationship between parameters α and *m* displays a parabola-shaped curve with a peak value (Fig. 2): α increases with *m* on the left side of the peak, and the trend is reversed on the right side of the peak. Our analysis showed that on the left side, a + 10% error in θ_{fc} caused a − 16.7% error in the estimated α value and a − 17.0% error in the estimated *m* value. On the right side, a + 10% error in θ_{fc} caused a 7.4% error in the α value and a − 3.3% error in the *m* value. The larger the error in the θ_{fc} value, the greater the errors in the corresponding α and *m* values.

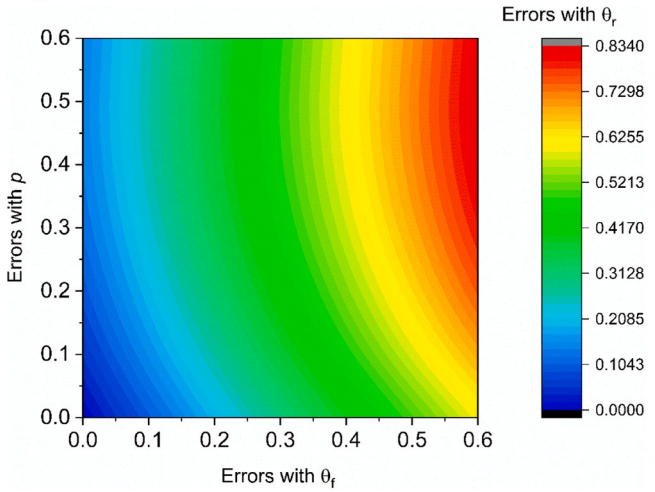

Fig. 4. The sensitivity of residual water content (θ_r) estimated using Eq. (9) to errors in both θ_f and *p*.

4.2. Evaluation of the new approach on repacked soil cores

Fig. 5 compares the new approach estimated SWRCs (solid lines) and the measured SWRCs (circles) for Soils 1–15. Generally, the new approach captured the variations of θ with *h* as affected by soil texture and ρ_b, as indicated by the relatively low values of bias (−0.047 to

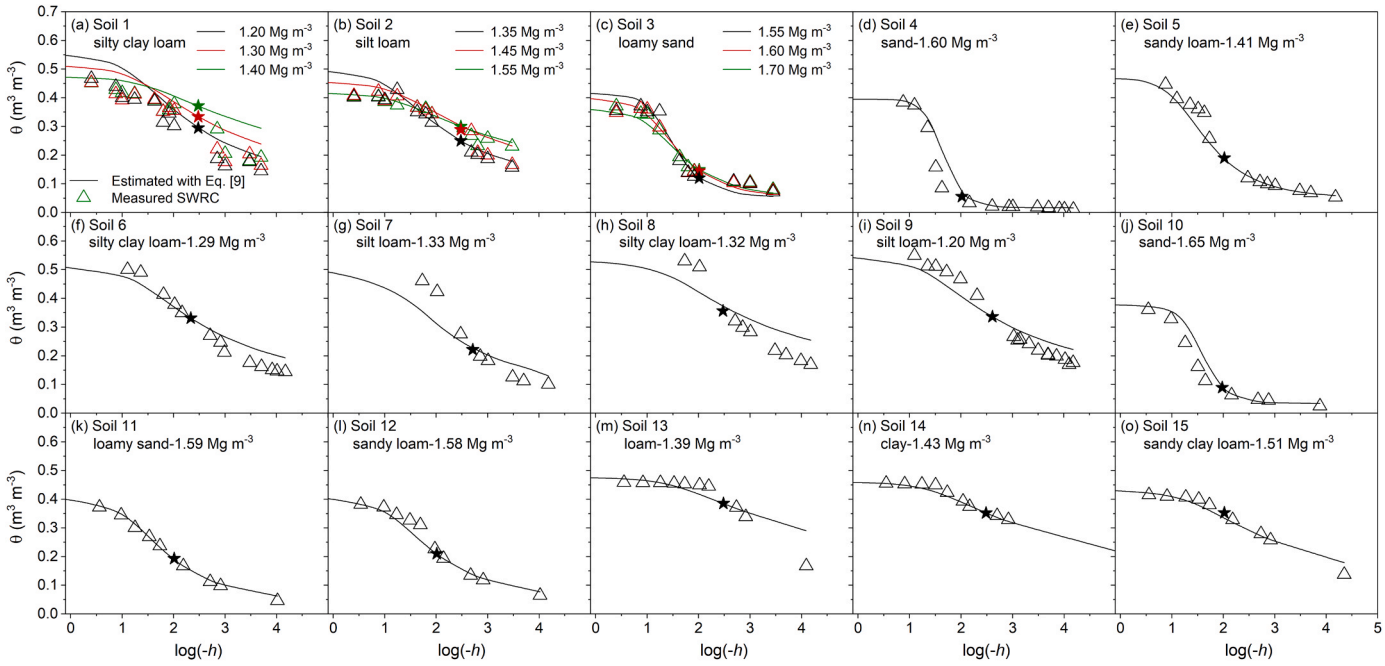

Fig. 5. Estimated soil water retention curves for soils 1–15 using the new approach (solid lines) compared with corresponding measured data (triangles), where θ is soil water content and log(-*h*) is the log of the absolute value of the soil water matric potential (*h*). The stars indicate the measured matching points used in the new approach calculations.

0.020 m^3 m^{-3}, with a mean value of −0.022 m^3 m^{-3}) and RMSE (0.014–0.079 m^3 m^{-3}, with a mean value of 0.045 m^3 m^{-3}), and relatively large values of coefficients of determination (R^2 = 0.84–0.99, with a mean value of 0.92) (Table 2).

Some discrepancies were observed between the measured and estimated SWRCs of the repacked soil cores. The new approach tended to overestimate θ values at the wet end, especially in soils with low ρ_b values. A source of error that contributed to the overestimations was the assumption that θ_s was equal to soil porosity (Eq. (2)). In practice, due to the presence of entrapped air, measured θ_s values are generally about 5–10% lower than soil porosity values (van Genuchten et al., 1991).

For several of the fine-textured soils (e.g., Soils 1, 6–9, and 13–15), the new approach overestimated θ values in the dry range, i.e., the estimated θ_r values were greater than the measured ones (Fig. 3(b), Fig. 5). In this study, we used Eq. (3) to estimate parameter θ_r by using the Lu et al. (2007) λ model (Eq. (10)), which sets parameter B as 0.96 and 0.27 for coarse- and fine-textured soils, respectively. Thus, uncertainties in parameter B led to errors in θ_f and *p*, which might have caused uncertainties in estimated θ_r values. Our analysis showed that for fine-textured soils, the constant B value of 0.27 produced an overestimated slope at the inflection point of the λ(θ) curve (i.e., ($\theta_{i\text{-}\lambda}$, λ_i) in Fig. 1). Lu and Dong (2015) also showed that the Lu et al. (2007) λ model gave overestimated λ values at intermediate water contents. Overestimated slope values produce greater θ_f and *p* values, which result in overestimated θ_r values (Eq. (9)).

Compared to the measured SWRCs in the log(-*h*) range of 1.5–2.5, the new approach underestimated θ values, and the estimated SWRCs had lower slopes (-dθ/d(-*h*)) in some soils (e.g., Soils 7–9). This phenomenon could have resulted from inaccurate *m* and α information due to errors in the θ_{fc} values. For these soils, the model parameter *m* was located on the right side of the peak value in the parabola-shaped curve of Eq. (13). Underestimated *m* values or overestimated α values occurred when positive errors were associated with the inputs of θ_{fc} (Figs. 3(c) and 3(d)).

Table 2
The bias, root mean square error (RMSE), and best fit coefficients of determination (R^2) for the new approach estimated soil water retention curves for Soil 1–23.

Sample type	Soil Code	Texture	bias	RMSE	R^2
			m^3 m^{-3}		
Repacked soil cores	1	silty clay loam	-0.060	0.068	0.89
	2	silt loam	-0.019	0.030	0.92
	3	loamy sand	-0.003	0.024	0.96
	4	sand	-0.026	0.052	0.91
	5	sandy loam	0.012	0.028	0.97
	6	silty clay loam	-0.015	0.034	0.99
	7	silt loam	0.008	0.058	0.97
	8	silty clay loam	-0.008	0.056	0.98
	9	silt loam	-0.001	0.039	0.97
	10	sand	-0.031	0.050	0.93
	11	loamy sand	-0.011	0.015	0.99
	12	sandy loam	0.008	0.020	0.97
	13	loam	0.000	0.041	0.84
	14	clay	0.012	0.025	0.95
	15	sandy clay loam	0.011	0.018	0.96
	Mean		-0.017	0.042	0.91
Intact soil cores	1(N)	silty clay loam	0.000	0.017	0.96
	1(R)	silty clay loam	0.001	0.032	0.93
	2	silt loam	0.001	0.036	0.95
	3	loamy sand	0.001	0.032	0.95
	16	Fontainebleau sand	-0.029	0.039	0.97
	17	Avignon silty clay loam	-0.010	0.017	0.98
	18	Collias loam	-0.017	0.027	0.96
	19	silt loam	-0.020	0.038	0.97
	20	silt	-0.016	0.042	0.94
	21	silt clay	-0.009	0.015	0.98
	22	loam	0.003	0.006	1.00
	23	clay	0.009	0.021	0.98
	Mean		-0.013	0.030	0.95
Field measurement	1	clay loam	0.007	0.049	0.81

4.3. Evaluation of the new approach to estimate SWRCs of intact soil cores

Fig. 6 presents comparisons of intact soil core estimated SWRCs using the new approach (solid lines) and measured SWRCs (circles). Several soil cores with different ρ_b values were collected at different depths of Soil 1 (under treatments N and R), Soil 2, and Soil 3. The estimated SWRCs generally agreed well with the measurements for all soils, depths, and tillage treatments. The RMSE and bias of the estimated SWRCs ranged from 0.009 to 0.062 $m^3\ m^{-3}$ (with a mean of 0.029 $m^3\ m^{-3}$) and − 0.044–0.15 $m^3\ m^{-3}$ (with a mean of −0.070 $m^3\ m^{-3}$), and the coefficient of determination of the fitted curve ranged from 0.93 to 0.99 (with a mean of 0.95) (Table 2).

Similar to the results obtained on repacked soil columns, the new approach slightly overestimated intact soil core water contents in the wet range of Soils 1–3, 16, 18, and 23, especially for samples with low ρ_b values. In particular, on Soil 1(R) with a ρ_b of 0.98 Mg m^{-3}, the estimated θ values in the wet range (log(-*h*) < 2) were significantly higher than the measured values. This was caused by the fact that θ_s was assumed to be equal to the total soil porosity. On Soils 18–20, the new approach slightly overestimated θ in the dry range (i.e., log(-*h*) > 2), which was attributed to the overestimated θ_r values, a phenomenon that also occurred on the repacked soil cores.

4.4. Evaluation of the new approach for estimating SWRCs of field soil

Field soil dynamics of θ and *h* at the 10-cm depth in Soil 1 were measured from DOY 150 to 234 (Fig. 7). During this period, the ρ_b varied between 1.26 and 1.40 Mg m^{-3}, *h* and θ values increased rapidly when rainfall occurred, and then decreased as the soil dried. The *h* values ranged from − 1800 to − 0.10 kPa, and the corresponding θ values varied from 0.08 to 0.44 $m^3\ m^{-3}$.

The θ values were calculated from measured *h* values using estimated model parameters (Fig. 2). Parameter θ_s was obtained with Eq. (2) using the ρ_s and ρ_b values. Parameters θ_f and *p* were estimated by solving Eqs. (4) and (10) using PSD and ρ_b data, which were used to calculate the θ_r value with Eq. (9). Finally, parameters α and *m* were estimated by solving Eqs. (13) and (14) simultaneously using the θ_s, θ_r, and measured θ_{fc} value.

Comparisons between the estimated and measured θ values showed that the new approach was able to capture the temporal dynamics of field water content, with a RMSE of 0.049 $m^3\ m^{-3}$ and a bias of 0.0070 $m^3\ m^{-3}$ (Fig. 7(b), Table 2). However, some estimated data did deviate from the measured θ curves, especially when soil θ was relatively large after rainfall. For example, on DOY 187 when the soil had a ρ_b value of 1.35 Mg m^{-3}, *h* increased from − 1400 kPa to − 0.10 kPa, and θ increased from 0.11 $m^3\ m^{-3}$ to 0.33 $m^3\ m^{-3}$ in response to a 42-mm rainfall. Accordingly, the estimated θ value increased from 0.10 $m^3\ m^{-3}$ to 0.49 $m^3\ m^{-3}$, which overestimated θ in the wet region. The difference between estimated and measured θ values in wet soil conditions could result from (1) the assumption that θ_s was equivalent to soil porosity, which is rare under field condition due to the presence of entrapped air; (2) the difference between the sensing ranges of Tensiomark (varies with soil water content) and the TDR sensors (about 29.7 cm^3, Peng et al., 2019); (3) compared to TDR sensors, Tensiomark sensors are more likely to disturb the soil, and it is necessary to cover the Tensiomark sensor with soil before installation; (4) Tensiomark sensors are less sensitive to water content changes compared to TDR sensors; and (5) the fact that θ measurement frequency (4 h) might not accurately capture the rapid θ changes after a rainfall event.

Other factors could also have contributed uncertainties to the estimated SWRCs. First, the *h* values from the TensioMark sensors were

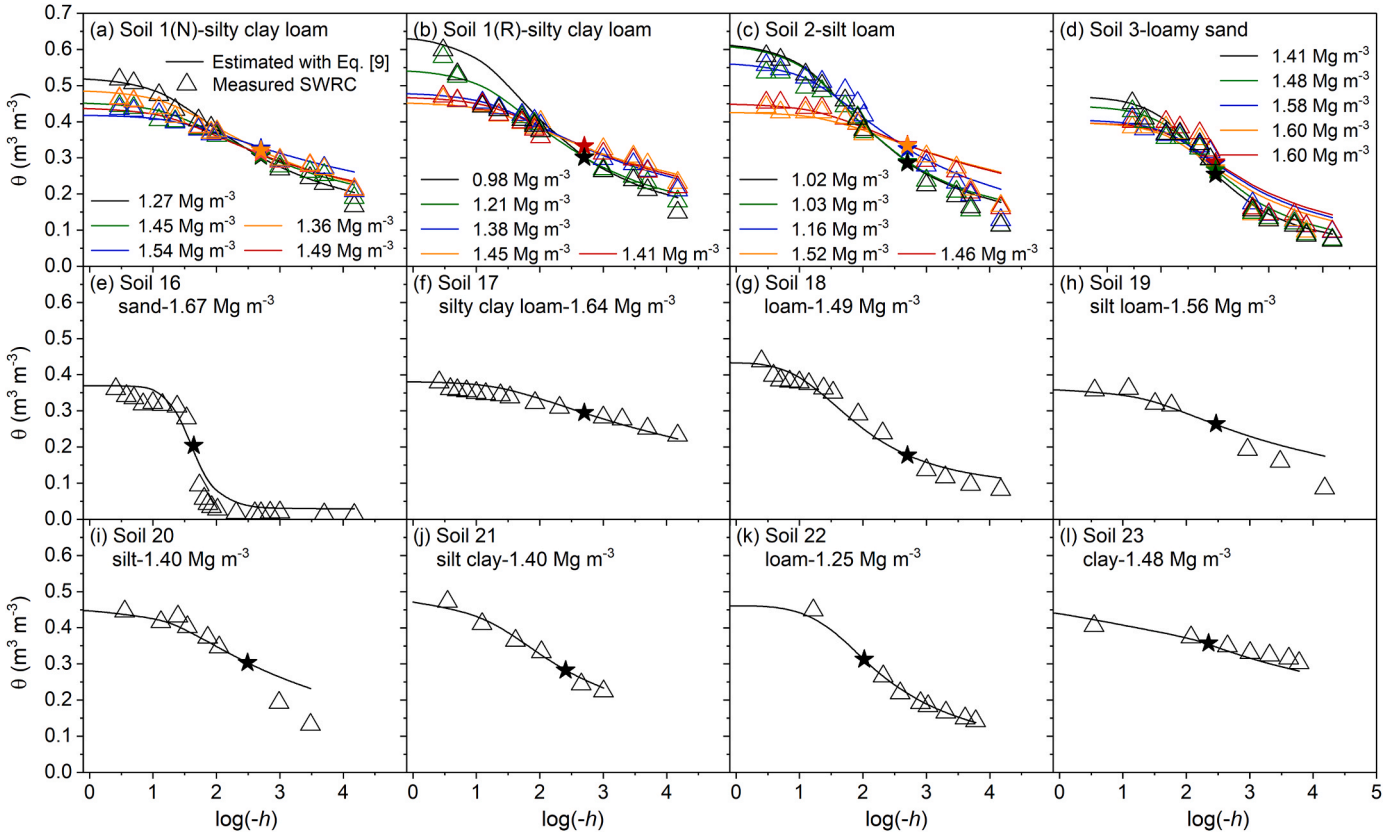

Fig. 6. Estimated soil water retention curves (solid lines) of soils 1–3 and 16–23 compared to the corresponding measured values (triangles), where θ is soil water content and log(-*h*) is the log of the absolute value of soil water matric potential (*h*). The stars represent the measured matching points used for the new approach calculations.

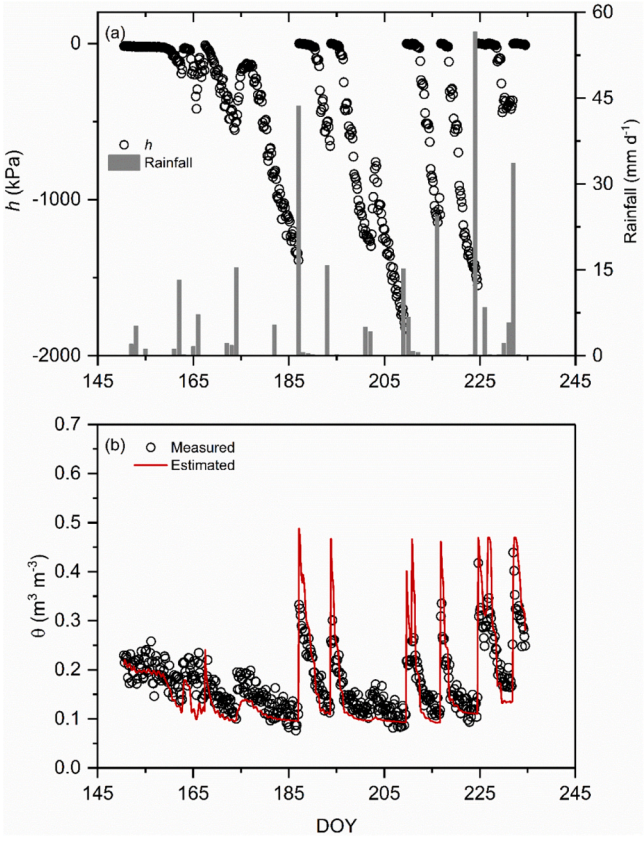

Fig. 7. Observed (circles) and estimated (solid curves) temporal variations of (a) soil matric potential (*h*), rainfall, and (b) water content (θ) at the 10-cm depth of field Soil 1 from DOY 150–234, 2020.

sensitive to soil temperature, soil-sensor contact, and structural changes caused by swelling/shrinking during wetting/drying processes (Bruand et al., 1996; Sun et al., 2009; Bonder et al., 2013; Zhang et al., 2017). Second, the θ-*h* relationship could differ between wetting and drying (i.e., the hysteresis phenomenon) (Bottraud and Rhoades, 1985), which inevitably manifested under field conditions. Finally, the new approach used to derive SWRC model parameters was based on a graphical method, which involved empirical approximations, and thus, had inherent limitations.

4.5. Limitations of the new approach in estimating SWRCs

Although the new approach produced accurate θ values with RMSEs of 0.042, 0.030, and 0.049 $m^3\ m^{-3}$ on repacked soils, intact soils, and field measurements, respectively (Table 2), it required a measured θ value at field capacity (−33 kPa or −10 kPa) as an input. Future research should focus on estimating θ_{fc} from intrinsic soil physical properties. Finally, the new approach might be improved by further exploring the relationships between the van Genuchten SWRC model parameters and the Lu and Dong (2015) λ model parameters, especially how these parameters vary with soil texture, bulk density, and structure.

5. Conclusion

In this study, a new approach was developed to estimate van Genuchten (1980) SWRC model parameters (θ_s, θ_r, α, *m*) from the thermal conductivity curve, soil texture, bulk density, and water content at field capacity. The new approach was evaluated using measurements on repacked soil cores, intact soil cores, and in situ field soil observations. The results showed that the new approach produced accurate SWRC estimates over the entire matric potential range, with root mean square errors less than 0.05 $m^3\ m^{-3}$. The approach developed herein has the potential to estimate SWRCs from basic soil properties and thermal conductivity curves that can be easily measured in the field.

Declaration of Competing Interest

The authors declare that there is no conflict of interest regarding the publication of this article.

Data availability

Data will be made available on request.

Acknowledgements

This research was supported by The Nature Conservancy (P120473), the National Natural Science Foundation of China (41977011), and the U.S. National Science Foundation (2037504) and USDA-NIFA Multi-State Project 4188. We would like to appreciate the valuable comments from the Editor and Reviewers.

Appendix A. Determining $\theta_{i\lambda}$, λ_i, and λ_r values using the Lu and Dong (2015) λ model

The first- and the second-order derivative of Eq. (4) can be obtained by differentiating Eq. (4) along the λ(θ) curve, resulting in the slope at a point on the λ(θ) curve (λ') and the curvature relationship (λ'') as follows,

$$\lambda' = \frac{d\lambda}{d\theta} = \left(\lambda_{sat} - \lambda_{dry}\right)\frac{p}{1-p}\theta_f^{\frac{1}{p-1}}\theta^{\frac{p}{1-p}}\left[1+\left(\frac{\theta}{\theta_f}\right)^{\frac{1}{1-p}}\right]^{-1-p} \tag{A1}$$

$$\lambda'' = \frac{dS_\lambda}{d\theta} = \left(\lambda_{sat} - \lambda_{dry}\right)\frac{p\theta_f^{\frac{1}{p-1}}\theta^{\frac{2p-1}{1-p}}\left[1+\left(\frac{\theta}{\theta_f}\right)^{\frac{1}{1-p}}\right]^{-2-p}\left\{p\left(1+\left(\frac{\theta}{\theta_f}\right)^{\frac{1}{1-p}}\right)-(1+p)\left(\frac{\theta}{\theta_f}\right)^{\frac{1}{1-p}}\right\}}{(1-p)^2} \tag{A2}$$

The θ value at the inflection point of the λ(θ) curve ($\theta_{i\lambda}$) can be computed by solving the second-order derivative with λ'' = 0,

$$\theta_{i-\lambda} = \theta_f p^{1-p} \tag{A3}$$

Then, its corresponding value, λ_i, can be derived by substituting Eq. (A3) into Eq. (4),

$$\lambda_i = \lambda_{dry} + \left(\lambda_{sat} - \lambda_{dry}\right)\left[1-(1+p)^{-p}\right] \tag{A4}$$

and the λ value at the residual water content (λ_r) also can be expressed as,

$$\lambda_r = \lambda_{dry} + (\lambda_{sat} - \lambda_{dry})\left\{1 - \left[1 + \left(\frac{\theta_r}{\theta_f}\right)^{\frac{1}{1-p}}\right]^{-p}\right\} \tag{A5}$$

Thus, the slope at the inflection point of λ(θ) curve (λ_i') can be expressed as,

$$\lambda_i' = \frac{d\lambda_i}{d\theta_{i\lambda}} = (\lambda_{sat} - \lambda_{dry})\frac{p^{p+1}}{(1+p)^{1+p}(1-p)}\theta_f^{-1} \tag{A6}$$

and,

$$\lambda_i' = \frac{\lambda_i - \lambda_r}{\theta_{i\lambda} - \theta_r} = \frac{(\lambda_{sat} - \lambda_{dry})\left\{\left[1 + \left(\frac{\theta_r}{\theta_f}\right)^{\frac{1}{1-p}}\right]^{-p} - (1+p)^{-p}\right\}}{\theta_f p^{1-p} - \theta_r} \tag{A7}$$

Combining Eqs. (A6) and (A7), enables the θ_r value to be derived from,

$$\left[1 + \left(\frac{\theta_r}{\theta_f}\right)^{\frac{1}{1-p}}\right]^{-p} = (1+p)^{-p} + (\theta_f p^{1-p} - \theta_r)\left(\frac{p}{1+p}\right)^{p+1}\frac{\theta_f^{-1}}{1-p} \tag{A8}$$

Appendix B. Determining the slope of the SWRC

Differentiating Eq. (1) once and twice along the SWRC curve results in its first- and second-order derivatives,

$$\theta' = \frac{d\theta}{d(\log(-h))} = \frac{d\theta}{dh}\frac{dh}{d(\log(-h))} = -mn\ln(10)(\theta_s - \theta_r)(-\alpha h)^n[1 + (-\alpha h)^n]^{-1-m} \tag{B1}$$

$$\theta'' = \frac{dS_h}{d(\log(-h))} = \frac{\frac{d\theta}{d(\log(-h))}}{dh}\frac{dh}{d(\log(-h))} \tag{B2}$$

$$= -mn^2[\ln(10)]^2(\theta_s - \theta_r)(-\alpha h)^n[1 + (-\alpha h)^n]^{-2-m}[1 - m(-\alpha h)^n]$$

Thus, for a SWRC, the value of θ and the corresponding log(-*h*) value at the inflection point (the point where the modulus of slope reaches its maximum) θ_{ih} and log(-h_i) can be expressed as,

$$\theta_{ih} = \theta_r + (\theta_s - \theta_r)\left(1 + \frac{1}{m}\right)^{-m} \tag{B3}$$

$$\log(-h_i) = -\log\alpha - \frac{1}{n}\log m \tag{B4}$$

Consequently, the slope at the inflection point of a SWRC is described as follows,

$$\theta_i' = \frac{d\theta}{d(\log(-h_i))} = -n(\theta_s - \theta_r)\frac{\ln(10)}{\left(1 + \frac{1}{m}\right)^{m+1}} \tag{B5}$$

and,

$$\theta_i' = \frac{\theta_s - \theta_{ih}}{\log(-h_a) - \log(-h_i)} = \frac{(\theta_s - \theta_r)\left[1 - \left(1 + \frac{1}{m}\right)^{-m}\right]}{\log(-h_a) + \log\alpha + \frac{1}{n}\log m} \tag{B6}$$

where -h_a is the air-entry matric potential value.

Appendix C. Determining bulk column *h* from measured values at a specific depth

Generally, the matric potential *h* is,

$$h = \frac{P}{\rho_w g} \tag{C1}$$

where *P* is the capillary pressure, ρ_w is the density of water (1 g cm^{-3}), *g* is the acceleration due to gravity (9.8 m s^{-2}).

The *P* value at a specific elevation (*z*) is equal to the pressure difference between the nonwetting fluid (air, P_a) and the wetting fluid (water, P_w) (Jalbert and Dane, 2001),

$$P(z) = P_a(z) - P_w(z) \tag{C2}$$

Thus, the representative matric potential ($\overline{h}$) over the height of the sample is (Jalbert and Dane, 2001),

$$\overline{h} = \frac{\overline{P}}{\rho_w g} = \frac{\overline{P}_a - \overline{P}_w}{\rho_w g} \tag{C3}$$

where $\overline{P}$, $\overline{P_w}$, and $\overline{P_a}$ are the representative values over the height of the sample on soil, water, and air, respectively.

At equilibrium, the P_w and P_a values at depth z above the bottom of the sample are,

$$P_w(z) = \overline{P}_w - \rho_w g(z - z_w) \tag{C4}$$

$$P_a(z) = \overline{P}_a - \rho_a g(z - z_a) \tag{C5}$$

where ρ_a is the density of air (0.00129 g cm^{-3}), z_w and z_a are the elevations at which the P_w and P_a are determined. Combining Eqs. (C1–C5), $\overline{h}$ is expressed as,

$$\overline{h} = h - \frac{\rho_a}{\rho_w} z_a + z_w - \left(1 - \frac{\rho_a}{\rho_w}\right) z \tag{C6}$$

In our experiment, the reference depth was the bottom of soil sample, thus, $z_a = 5$ cm, $z_w = 0$ cm, and $z = 2.5$ cm. Then the $\overline{h}$ values were calculated from measured h data using Eq. (C6).

References

Arya, L.M., Paris, J.F., 1981. A physicoempirical approach to predict the soil water moisture characteristic from particle size distribution and bulk density data. Soil Sci. Soc. Am. J. 45, 1023–1030.

Assouline, S., 2004. Rainfall-induced soil surface sealing: a critical review of observations, conceptual models, and solutions. Vadose Zone J. 3, 570–591.

Assouline, S., Or, D., 2014. The concept of field capacity revisited: defining intrinsic static and dynamic criteria for soil internal drainage dynamics. Water Resour. Res. 50, 4787–4802.

Bittelli, M., Flury, M., 2009. Errors in water retention curves determined with pressure plates. Soil Sci. Soc. Am. J. 73, 1453–1460.

Bonder, G., Scholl, P., Loiskandl, W., Kaul, H.P., 2013. Environmental and management influences on temporal variability of near saturated soil hydraulic properties. Geoderma 204, 120–129.

Børgesen, C.D., Iversen, B.V., Jacobsen, O.H., Schaap, M.G., 2008. Pedotransfer functions estimating soil hydraulic properties using different soil parameters. Hydrol. Process. 22, 1630–1639.

Bottraud, J.C., Rhoades, J.D., 1985. Referencing water content effects on soil electrical conductivity-salinity calibrations. Soil Sci. Soc. Am. J. 49, 1579–1581.

Brooks, R.H., Corey, A.T., 1964. Hydraulic properties of porous media. Hydrology papers 3. Colorado State University.,, Fort Collins, CO, pp. 1–27.

Bruand, A., Cousin, I., Nicoullaud, B., Duval, O., Begn, J.C., 1996. Backscattered electron scanning images of soil porosity for analyzing soil compaction around roots. Soil Sci. Soc. Am. J. 60, 895–901.

Chen, C., Hu, K.L., Liu, G., 2014. Estimating the wet-end section of soil water retention curve by using the dry-end section. Soil Sci. Soc. Am. J. 78, 1878–1883.

Colman, E., 1947. A laboratory procedure for determining the field capacity of soils. Soil Sci. 63, 277–284.

Dane, J.H., Hopmans, J.W., 2002. Water retention and storage. In: Dane, J.H., Topp, G.C. (Eds.), Methods of Soil Analysis. Physical Methods. Part. 4. SSSA, Madison, WI, pp. 671–796.

Doussan, C., Ruy, S., 2009. Prediction of unsaturated soil hydraulic conductivity with electrical conductivity. Water Resour. Res. 45, 1–12.

Ewing, R., Horton, R., 2007. Thermal conductivity of a cubic lattice of spheres with capillary bridges. J. Phys. D. -Appl. Phys. 40, 4959–4965.

Ewing, R.P., Ghanbarian, B., Hunt, A.G., 2015. Gradients and assumptions affect interpretation of laboratory-measured gas-phase transport. Soil Sci. Soc. Am. J. 79, 1018–1029.

Fredlund, D.G., Xing, A., 1994. Equations for the soil-water characteristic curve. Can. Geotech. J. 31, 521–532.

Fu, X.L., Shao, M.A., Lu, D.Q., Wang, H.M., 2011. Soil water characteristic curve measurement without bulk density changes and its implications in the estimation of soil hydraulic properties. Geoderma 167, 1–8.

Fu, Y.W., Horton, R., Ren, T.S., Heitman, J.L., 2021a. A general form of Archie's model for estimating bulk soil electrical conductivity. J. Hydrol. 597, 126160.

Fu, Y.W., Lu, S., Ren, T.S., Horton, R., Heitman, J.L., 2021b. Estimating soil water retention curves from soil thermal conductivity measurements. J. Hydrol. 603, 127171.

Gardner, W.R., Hillel, D., Benyamini, Y., 1970. Post-irrigation movement of soil water. 1. Redistribution. Water Resour. Res. 6, 851–861.

Gee, G.W., Or, D., 2002. Particle-size analysis. In: Dane, J.H., Topp, G.C. (Eds.), Methods of Soil analysis. Physical Methods. SSSA Book Ser. 5. Part. 4. SSSA, Madison, WI, pp. 255–293.

Ghanbarian, B., Hunt, A.G., Skinner, T.E., Ewing, R.P., 2015. Saturation dependence of transport in porous media predicted by percolation and effective medium theories. Fractal.: Interdiscip. J. Complex Geom. Nat. 23, 1540004.

Gupta, S.C., Larson, W.E., 1979. Estimating soil water retention characteristics from particle size distribution, organic matter content and bulk density. Water Resour. Res. 15, 1633–1635.

He, H.L., Dyck, M., Lv, J.L., 2020. A new model for predicting soil thermal conductivity from matric potential. J. Hydrol. 589, 125167.

Hunt, A.G., Ewing, R.P., Horton, R., 2013. What's wrong with soil physics? Soil Sci. Soc. Am. J. 77, 1877–1887.

Jalbert, M., Dane, J.H., 2001. Correcting laboratory retention curves for hydrostatic fluid distributions. Soil Sci. Soc. Am. J. 65, 648–654.

Jensen, D.K., Tuller, M., de Jonge, L.W., Arthur, E., Moldrup, P., 2015. A new two-stage approach to predicting the soil water characteristic from saturation to oven-dryness. J. Hydrol. 521, 498–507.

Johansen, O., 1975. Thermal Conductivity of Soils (Ph.D. diss). Norwegian Univ. of Science and Technology,, Trondheim.

Kirkham, M.B., 2005. Principles of Soil and Plant Water Relations. Elsevier Academic Press,, Amsterdam, San Diego, California, p. 500.

Kroener, E., Campbell, G.S., Bittelli, M., 2018. Estimation of thermal instabilities in soils around underground electrical power cables. Vadose Zone J. 16.

Likos, W.J., 2014. Modeling thermal conductivity dryout curves from soil-water characteristic curves. J. Geotech. Geoenviron. Eng. 140.

Lu, N., Dong, Y., 2015. Closed-form equation for thermal conductivity of unsaturated soils at room temperature. J. Geotech. Geoenviron. Eng. 141, 04015016.

Lu, N., Likos, J.W., 2004. Unsaturated Soil Mechanics. Wiley,, Hoboken, NJ.

Lu, S., Ren, T., Gong, Y., Horton, R., 2007. An improved model for predicting soil thermal conductivity from water content. Soil Sci. Soc. Am. J. 71, 8–14.

Lu, S., Ren, T., Gong, Y., Horton, R., 2008. Evaluation of three models that describe soil water retention curves from saturation to oven dryness. Soil Sci. Soc. Am. J. 72, 1542–1546.

Lu, S., Lu, Y.L., Peng, W., Ju, Z.Q., Ren, T.S., 2019. A generalized relationship between thermal conductivity and matric suction of soils. Geoderma 337, 491–497.

McCumber, M.C., Pielke, R.A., 1981. Simulation of the effects of surface fluxes of heat and moisture in a mesoscale numerical model: 1. Soil layer. J. Geophys. Res. -Oceans 86, 9929–9938.

Miller, E.E., Klute, A., 1967. The dynamics of soil water: I. Mechanical forces. In: Hagan, R.M., et al. (Eds.), Irrigation of Agricultural Lands. America Society of Agronom, Madison, WI, pp. 209–244.

Minasny, B., McBratney, A.B., Bristow, K.L., 1999. Comparison of different approaches to the development of pedotransfer functions for water-retention curves. Geoderma 93, 225–253.

Mohammadi, M.H., Vanclooster, M., 2011. Predicting the soil moisture characteristic curve from particle size distribution with a simple conceptual model. Vadose Zone J. 10, 594–602.

Nemes, A., Schaap, M.G., Leij, F.J., 1999. The UNSODA Unsaturated Soil Hydraulic Database. U.S. Salinity Lab.,, Riverside, CA.

Nichol, C., Smith, L., Beckie, R., 2003. Long-term measurement of matric suction using thermal conductivity sensors. Can. Geotech. J. 40, 587–597.

Nitao, J.J., Bear, J., 1996. Potentials and their role in transport in porous media. Water Resour. Res. 32 (2), 225–250.

Peng, W., Lu, Y.L., Xie, X.T., Ren, T.S., Horton, R., 2019. An improved thermo-TDR technique for monitoring soil thermal properties, water content, bulk density, and porosity. Vadose Zone J. 18, 190026.

Poeplau, C., Eriksson, J., Katterer, T., 2015. Estimating residual water content in airdried soil from organic carbon and clay content. Soil Tillage Res. 145, 181–183.

Pozdnyakov, A.I., Pozdnyakova, L.A., Karpachevskii, L.O., 2006. Relationship between water tension and electrical resistivity in soils. Eurasia Soil Sci. 39 (1 Supplement), S78–S83.

Reece, C.F., 1996. Evaluation of a line heat dissipation sensor for measuring soil matric potential. Soil Sci. Soc. Am. J. 60, 1022–1028.

Schaap, M.G., Leij, F.J., 1998. Using neural networks to predict soil water retention and soil hydraulic conductivity. Soil Tillage Res. 47, 37–42.
Schaap, M.G., Leij, F.J., 2000. Improved prediction of unsaturated hydraulic conductivity with the Mualem-van Genuchten model. Soil Sci. Soc. Am. J. 64, 843–851.
Schelle, H., Heise, L., Jänicke, K., Durner, W., 2013. Water retention characteristics of soils over the whole moisture range: a comparison of laboratory methods. Eur. J. Soil Sci. 64, 814–821.
Sun, Y., Lin, J., Lammers, P.S., Damerow, L., Hueging, H., Zhang, H., Sun, W., 2009. Predicting surface porosity using a fine-scale index of roughness in a cultivated field. Soil Tillage Res. 103, 57–64.
Tian, Z., Gao, W., Kool, D., Ren, T., Horton, R., Heitman, J.L., 2018. Approaches for estimating soil water retention curves at various bulk densities with the extended van Genuchten model. Water Resour. Res. 54, 5584–5601.
Tuller, M., Or, D., 2005. Water films and scaling of soil characteristic curves at low water contents. Water Resour. Res. 41, W09403.
van Genuchten, M.T., 1980. A closed-form equation for predicting the hydraulic conductivity of unsaturated soils. Soil Sci. Soc. Am. J. 44, 892–898.
van Genuchten, M.T., Leij, F.J., Yates, S.R., 1991. The RETC Code for Quantifying the Hydraulic Functions of Unsaturated Soils (EPA/600/2-91/065). US Environmental Protection Agency,, Ada, OK.
Veihmeyer, F.J., Hendrickson, A.H., 1931. The moisture equivalent as a measure of the field capacity of soils. Soil Sci. 32, 181–193.
Vogel, T., Cislerova, M., 1988. On the reliability of unsaturated hydraulic conductivity calculated from the moisture retention curve. Transp. Porous Media 3, 1–15.
Weynants, M., Vereecken, H., Javaux, M., 2009. Revisiting Vereecken pedotransfer functions: introducing a closed-form hydraulic model. Vadose Zone J. 8, 86–95.
Wösten, J.H.M., Lilly, A., Nemes, A., Bas, C.L., 1999. Development and use of a database of hydraulic properties of European soils. Geoderma 90, 169–185.
Yan, G.X., Bore, T., Schlaeger, S., Scheuermann, A., Li, L., 2022. Investigating scale effects in soil water retention curve via spatial time domain reflectometry. J. Hydrol. 612, 128238.
Zhai, Q., Rahardjo, H., 2012. Determination of soil-water characteristic curve variables. Comput. Geotech. 42, 37–43.
Zhang, M., Lu, Y., Heitman, J.L., Horton, R., Ren, T., 2017. Temporal changes of soil water retention behavior as affected by wetting and drying following tillage. Soil Sci. Soc. Am. J. 81, 1288–1295.